C. R. Physique 13 (2012) 207–217

Contents lists available at SciVerse ScienceDirect

Comptes Rendus Physique

www.sciencedirect.com

Use of large scale facilities for research in metallurgy

Study of the structure and physical properties of quasicrystals using large scale facilities

Étude de la structure et des propriétés physiques des quasi-cristaux par l'utilisation des grands instruments

Marc de Boissieu

Sciences de l'ingenierie, des materiaux et des procedes (SIMaP), Grenoble INP, CNRS, UJF, BP 75, 38402 St Martin d'Hères cedex, France

ARTICLE INFO

Article history:
Available online 28 January 2012

Keywords:
Quasicrystals
Long range order
Icosahedral quasicrystals

Mots-clés :
Quasicristaux
Ordre à longue distance
Quasicristaux icosaédriques

ABSTRACT

Quasicrystals have been puzzling scientists since their discovery. In this article we review some of the recent advances in this field and show how the use of large scale facilities has brought in decisive information for the understanding of their structure and physical properties.

RÉSUMÉ

Les quasicristaux ont intrigué les scientifiques depuis leur découverte. Dans cet article nous passons en revue certaines des avancées récentes dans ce domaine, et montrons comment l'utilisation des grands instruments a apporté des informations décisives pour la compréhension de leur structure et de leurs propriétés physiques.

1. Introduction

Quasicrystals have been puzzling the scientific community since their discovery by Shechtman et al. more than 25 years ago [1]. Indeed, their diffraction pattern presents extremely sharp Bragg peaks, as a signature of long range order, but with rotational symmetries, such as the icosahedral one, incompatible with lattice periodicity. Although the first quasicrystals were obtained by rapid quench from the melt, they can now be obtained as equilibrium phases in a few systems and grown as large single grains, using the Bridgman or the Czokralski technique. This is illustrated in Fig. 1 showing a single crystal in the ZnMgY system, with clear dodecahedral facets, and a 5-fold X-ray Laue diffraction pattern obtained with a single grain of the i-AlPdMn phase.

Large scale facilities have played a key role in the understanding of the structure and physical properties of quasicrystals. To illustrate this purpose, we present in this article a few examples taken from the study of icosahedral quasicrystals and, in particular, their atomic structure, phason modes and diffuse scattering and lattice dynamics. A detailed introduction to aperiodic crystals and quasicrystals can be found in the book [2].

E-mail address: Marc.de-boissieu@simap.inpg.fr.

1631-0705/$ – see front matter
doi:10.1016/j.crhy.2011.11.008

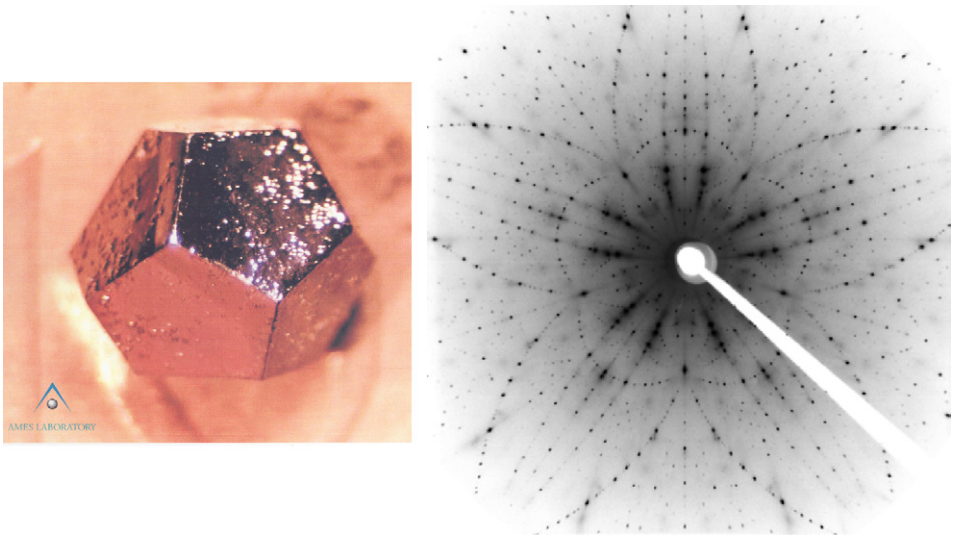

Fig. 1. Left panel: Single crystal obtained by the flux method in the Zn–Mg–Y system (Courtesy of P. Canfield [3]). Right panel: 5-fold Laue diffraction pattern obtained in the icosahedral AlPdMn phase (Courtesy of W. Steurer).

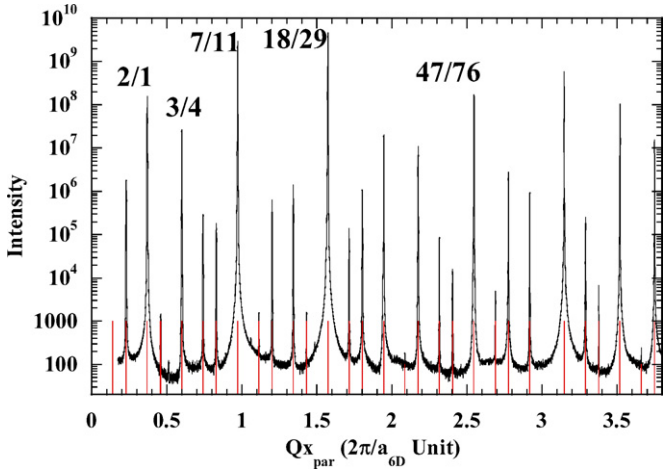

Fig. 2. Q-scan measured in the i-AlPdMn quasicrystal along a 5-fold axis. The measurement has been carried out on the D2AM beam line at the ESRF. The solid line corresponds to the measured intensity on a logarithmic scale. The horizontal axis corresponds to the Qx component of the reciprocal wavevector expressed in $2\pi/a_{6D}$ where a_{6D} is the 6D lattice parameter equal to about 6.451 Å. The vertical lines correspond to the ideal position of the Bragg peaks. A few Bragg peaks are labeled with a short-hand notation with 2 indices (N/M). Note the non-periodic distribution of the Bragg peaks, and the large dynamical range between the strongest and weakest Bragg peaks.

2. Atomic structure of icosahedral quasicrystals

The question 'where are the atoms in a quasicrystal?' has been puzzling researchers for many years. It is only recently that a satisfactory answer could be given to this fascinating question. Prior to a structural study being carried out, the problem of the structural quality of quasicrystal has to be addressed. It can be stated with the following question: 'how perfect is a quasicrystal?' Similarly to a periodic crystal, the quasicrystal perfection is best studied in reciprocal space. Two main points need to be considered: (i) the reciprocal space position of Bragg peaks must fulfill the quasicrystalline indexing scheme; and (ii) the Bragg peaks have to be as sharp as possible. In the case of icosahedral symmetry, the diffraction pattern of the quasicrystal can be indexed with a linear combination of six vectors pointing towards the vertices of an icosahedron. This six integer indexing is at the basis of the superspace representation of quasicrystal, here a six-dimensional (6D) superspace. The principle of this superspace crystallography is illustrated with the Fibonacci chain, a 1D quasicrystal, in Fig 3: the 1D quasicrystal can be obtained as a section of a 2D decorated lattice. For icosahedral quasicrystal, along a high symmetry direction, the indexing can be simplified to a linear combination of two collinear vectors whose lengths are in the ratio 1 and τ where τ is the golden mean defined as $\tau = (\sqrt{(5)} + 1)/2 = 1.618\ldots$. This is exemplified in Fig. 2, which displays a Q-scan measured along a 5-fold axis of the icosahedral AlPdMn quasicrystal. All Bragg peaks can be

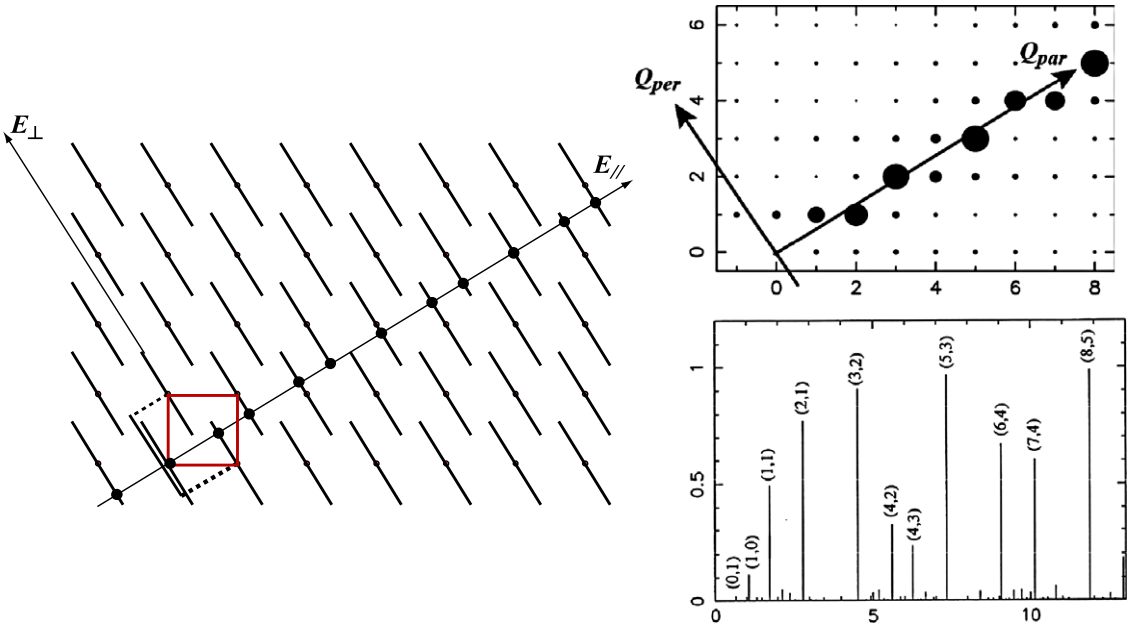

Fig. 3. Schematic representation of the superspace description of a 1D quasicrystal. Left: The 1D quasicrystal is obtained as a section through a decorated 2D lattice. Right: 2D diffraction pattern and its projection. The diffraction pattern can be indexed by 2 integer indices.

indexed using this linear combination. Note that the intensity scale is logarithmic, and that there is a large dynamical range between the strongest and weakest reflections.

The quasicrystalline model allows one to compute the 'ideal' position of the Bragg peaks shown as vertical bars in Fig. 2: as can be seen, there is a perfect match with the experiment. It is important to note that this is the only indexing solution and, for instance, indexing the diffraction pattern with a 3D periodic lattice would have been impossible, demonstrating that the diffraction pattern is quasiperiodic with an icosahedral symmetry.

Once the indexing is carried out, it is also important to study the shape and sharpness of Bragg reflections. This is again best achieved using a high resolution setup on a synchrotron radiation facility. Similarly to periodic crystal, the structural quality of the quasicrystal can be measured by the width of the Bragg reflection, from which a correlation length can be extracted. If highly perfect, the kinematical theory of diffraction no longer holds and the so-called dynamical effects are taking place. Such effects have indeed been observed in the i-AlPdMn quasicrystal demonstrating the high 'quality' of the quasiperiodic long range order which sets in, with a correlation length larger than 10 μm [4–6], similar to what is observed for the best periodic metallic alloys.

These experiments thus demonstrate without ambiguity that the long range quasiperiodic order in quasicrystal is a new kind of long range order.

It is only recently that a detailed understanding of the atomic structure was achieved for icosahedral phases.

The discovery of the binary $Cd_{5.7}Yb$ icosahedral quasicrystal has been a breakthrough, since it is the first binary quasicrystal, allowing thus a much simpler structural analysis [7]. Moreover, for chemical composition very close to the icosahedral one, a periodic approximant can be synthesized. In the high dimensional description this corresponds to a tilt of the E_{par} space until it reaches a rational slope approximating the golden mean. It can be equivalently expressed in term of a shear strain of the periodic lattice, the shear strain being in the perpendicular space direction: this is called a linear phason strain. The first rational approximations of $\tau = 1.618\ldots$ are 1/1 and 2/1, and the Cd_6Yb 1/1 and the $Cd_{5.8}Yb$ 2/1 approximants have been successfully synthesized. These are cubic phases, with a lattice parameter equal to 1.57 nm and 2.53 nm respectively. Their structures have been solved using standard crystallographic techniques and turned out to be simply described by a periodic packing of a large atomic cluster of diameter 1.57 nm and containing 158 atoms [8,9]. The large clusters are connected along their 2-fold axes, where they share a face, and along their 3-fold axes, where they overlap. The different shells constituting the cluster are shown in Fig. 4. Note that the shells are perfectly ordered chemically, Yb atoms sitting on the vertices of an icosahedron. The atomic structure of the icosahedral quasicrystal has been solved using data collected on the D2AM beam line of the ESRF synchrotron. This allowed the measurement of more than 5000 independent reflections with a large dynamical range of more than 7 orders of magnitudes. The measurement of a large number of weak Bragg peaks, only possible at synchrotron facilities, turned out to be an essential point in deriving a detailed structural model. Using these data, and the 6D superspace description of the quasicrystal, it could be shown that the structure of the icosahedral CdYb phase is built up with the same cluster, connected along the same 2-fold and 3-fold axis, but on a quasiperiodic lattice [10]. The distribution of the cluster centers in a 5-fold plane is shown in Fig. 4. As can be seen there is a hierarchical packing of the cluster: clusters are grouped in a 'cluster of clusters' forming a 10-fold ring highlighted in light grey, which themselves form an inflated cluster (large 10-fold ring of light grey disks).

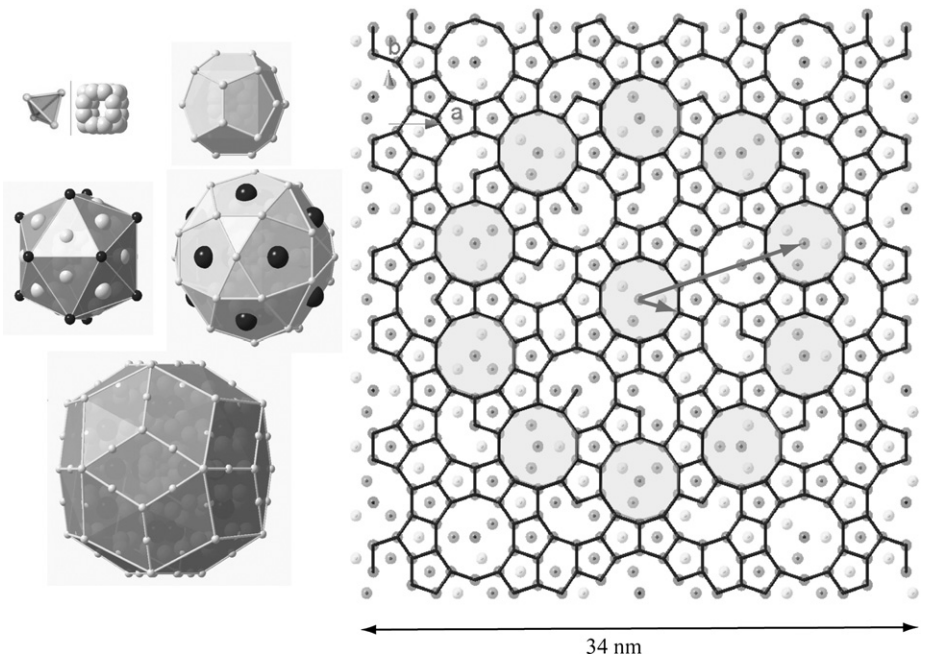

Fig. 4. Left panel: The successive shells making up the large triacontahedral cluster containing 158 atoms. Black spheres stand for Yb atoms. Right panel: Distribution of the cluster centers in a 5-fold plane. The light grey disk emphasizes a cluster of clusters (10-fold ring), which form an inflated cluster as shown by the two arrows (from [10]).

3. Diffuse scattering and phason modes

The name phasons was coined in 1971 by Overhauser [11] in the context of charge density wave (CDW) systems. Studying the lattice excitations of an incommensurate CDW, he demonstrated that because the free energy of the system is invariant under a phase shift of the modulation there are new lattice excitations which he named phasons, showing up around the satellite reflections and whose dispersion is acoustic like. The nature and damping of those modes has been intensely studied at a microscopical level in a few incommensurately modulated phases [12].

Soon after the discovery of quasicrystals, several groups pointed out the importance of phason modes [13–16]. Phason modes in quasicrystals are a consequence of the hydrodynamic theory, which applies for all aperiodic phases (for an introduction on phason modes see [17] and [2]). The underlying hypothesis relies on the invariance of the free energy of the system while moving the cut space along the perpendicular direction (see Fig. 3). Indeed the resulting structure which is obtained while moving the cut space is not identical, in general, to the initial one. However, its free energy is exactly the same. Using the long wavelength hydrodynamic approach it can be shown that this leads to long wavelength diffusive modes named phason modes. An elasticity theory of quasicrystals can then be derived, introducing the appropriate symmetry analysis. For the case of icosahedral phases, using group theory arguments it can be shown that the elastic free energy is the sum of three terms $F = F_{\text{par}} + F_{\text{per}} + F_{\text{par\_per}}$. The first term is proportional to the squared 'phonon' strain. It depends on the two Lamé coefficients λ and μ; because of the high symmetry of the icosahedral point group, this term is analogous to what is obtained for an isotropic solid. The second term is proportional to the squared 'phason' strain and depends on two phason elastic constants K1 and K2. Finally the third term depends on both the phonon and phason strain and on a phonon–phason coupling constant K3. Five elastic constants are thus required to account for the elasticity of icosahedral phases [13–15,18].

Based on the elasticity theory of icosahedral quasicrystals, the effect of equilibrium phonon and phason fluctuations on the diffraction pattern can be computed [19]. This follows the very same approach as the one used for computing the thermal diffuse scattering due to phonon, which can be found in the text book by Chaikin and Lubensky [20].

The scattered intensity at a point $\mathbf{Q}$ in reciprocal space can be written:

$$S(\mathbf{Q}) = S_{\text{Bragg}}(\mathbf{Q}) + S_{\text{Diff}}(\mathbf{Q}) \tag{1}$$

The first term correspond to the Bragg scattering, whereas the second one corresponds to the diffuse scattering originating from phonon and phason fluctuations. The diffuse scattering measured at the point $\mathbf{Q}_{\text{par}} + \mathbf{q}$, where $\mathbf{Q}_{\text{par}}$ is the position of a Bragg peak in the icosahedral diffraction pattern, can be computed within the hydrodynamic theory. If the phonon–phason coupling term can be neglected, the diffuse scattering intensity splits in two parts: the so-called thermal diffuse scattering (TDS) related to phonon and a second term corresponding to the phason modes contribution to the diffuse scattering, sometimes referred to as phason diffuse scattering (PDS).

Although the TDS and PDS parts share some similarities in their calculation, they lead to very different intensity distribution.

The thermal diffuse scattering intensity decays as $1/q^2$ along any given direction $\mathbf{q}$ from a Bragg peak positioned at $\mathbf{Q}$ having intensity $I_{\mathrm{Bragg}}(\mathbf{Q})$ and it scales as $I_{\mathrm{Bragg}}(\mathbf{Q}).Q_{\mathrm{par}}^2$. The elastic isotropy of the icosahedral symmetry yields a very recognizable thermal diffuse scattering intensity distribution around Bragg peaks having, whatever $\mathbf{Q}$, the shape of a 3D ellipsoid elongated in the two transverse directions to $\mathbf{Q}$.

The phason diffuse scattering intensity behaves differently and three major features allows one to identify it unambiguously [19]:

(i) the PDS intensity decays as $1/q^2$ along any given particular direction $\mathbf{q}$ from a Bragg peak positioned at $\mathbf{Q}$ having intensity $I_{\mathrm{Bragg}}(\mathbf{Q})$;
(ii) it scales as $I_{\mathrm{Bragg}}(\mathbf{Q}).Q_{\mathrm{per}}^2$;
(iii) the phason diffuse scattering intensity distribution is highly anisotropic around a given Bragg peak and it is different from one Bragg peak to another one as a consequence of the complex $\mathbf{q}$ dependence of the eigen-vectors $\mathbf{e}_{\mathrm{per},i}(\mathbf{q})$ and eigenvalues $\mathrm{K}_i(\mathbf{q}, \mathrm{K1}, \mathrm{K2})$ of the $C_{\mathrm{per,per}}(\mathbf{Q})$ matrix used to compute the diffuse scattering. It can be further stated that the anisotropy is mainly driven by the value of the ratio K2/K1 of the two phason elastic constants K1 and K2 which ranges between -0.60 and 0.75 in the icosahedral symmetry case. Whenever K2/K1 is negative and close to the lower limit value of -0.6, the phason diffuse scattering intensity is shown to be strengthened along directions parallel to three-fold axes around Bragg peaks whereas whenever it is positive and close to the upper limit value of $+0.75$, the strengthening occurs along directions parallel to five-fold axes around Bragg peak.

We stress here that all three above conditions must be experimentally checked so that the measured diffuse scattering signal can be unambiguously attributed to phason modes.

The evolution of the diffuse scattering with temperature and its relationship with phase transitions has also been studied within the Landau theory [21–23] when a phason strain is applied.

When measuring the diffuse scattering the TDS and PDS contribution might be difficult to disentangle. The situation is thus much simplified if the measurement contains only the PDS contribution. This can be achieved using elastic neutron scattering and an energy analysis which eliminates the TDS contribution. This is best realized on a triple axis instrument, preferably using a cold source which gives rise to a good Q and energy resolution. The measurement is then carried out at the elastic (zero energy transfer) position of the triple axis, ensuring that only the PDS contribution is measured. This is the best experimental solution, which, however, requires centimeter size single grain quasicrystal.

For measurements carried out at high temperature, that the TDS do not contribute to the scattered intensity is particularly important since the mean square atomic displacements $\langle u_{\mathrm{per}}^2 \rangle$ due to phonon modes grows as T in a first approximation and so does the TDS intensity.

When elastic neutron scattering is not feasible, diffuse X-ray scattering measurements carried out on an absolute scale are better suited. Absolute scale measurements have been widely used for the study of TDS and phonon modes in metals [24–30] and in the field of order–disorder transitions in metallic alloys [29]. The absolute scale measurements allows one to calculate the TDS contribution to the signal (if the elastic constants are known), to measure the phason elastic constant K1 and K2 on an absolute scale and more important, to compare different samples whatever the experimental configuration is.

To evidence the phason diffuse scattering in the i-AlPdMn icosahedral quasicrystal, neutron scattering experiment was carried out with an energy transfer analyzer and at the elastic position so that the TDS contribution is suppressed. Measurements have been carried out around a few Bragg reflections. The PDS intensity, being proportional to Q_{per}^2, reflections having different perpendicular components of their Bragg wave-vector have been studied in order to evidence this property relation.

Systematic diffuse intensity maps have been recorded around a few Bragg peaks and are shown in Fig. 5, where iso-intensity contours are plotted [31]. The same intensity scale has been selected for the four reflections, so that the different panels can be directly compared.

As can be seen in Fig. 5, the intensity distribution displays strong anisotropies. Several observations point towards a phason component for this diffuse scattering. First the 16/24 and 15/24 are two reflections having the same Bragg peak intensities, but with Q_{per} components in a ratio 3 to 1. As can be observed in Fig. 5(b, c), there is a much larger amount of diffuse scattering intensity around the 16/24 reflection, as expected. Second, the 18/29 and 16/24 reflections, are very close to each other in reciprocal space: any elastic (phonon) distortion would lead to a very similar shape of the diffuse scattering at the opposite of what is observed experimentally. This can be understood by computing the perpendicular component of these two reflections: they are almost orthogonal, and thus lead to a very different scalar product 'selection rule' in the PDS computation. Finally, measuring two collinear reflections, it is possible to show that the intensity of the diffuse scattering decays as q^{-2} and scales with the product $I_{\mathrm{Bragg}}.Q_{\mathrm{per}}^2$.

These results are confirmed by a computation of the diffuse scattering. If only phason fluctuations are contributing to the diffuse scattering intensity and if the coupling constant K3 is neglected, then the shape anisotropy depends only on the ratio K2/K1. Using the measured Bragg peaks intensity it is then possible to simulate the diffuse scattering as shown in Fig. 5(e–h), where a ratio $\mathrm{K2/K1} = -0.52$ has been used. As can be seen there is a good agreement between simulation

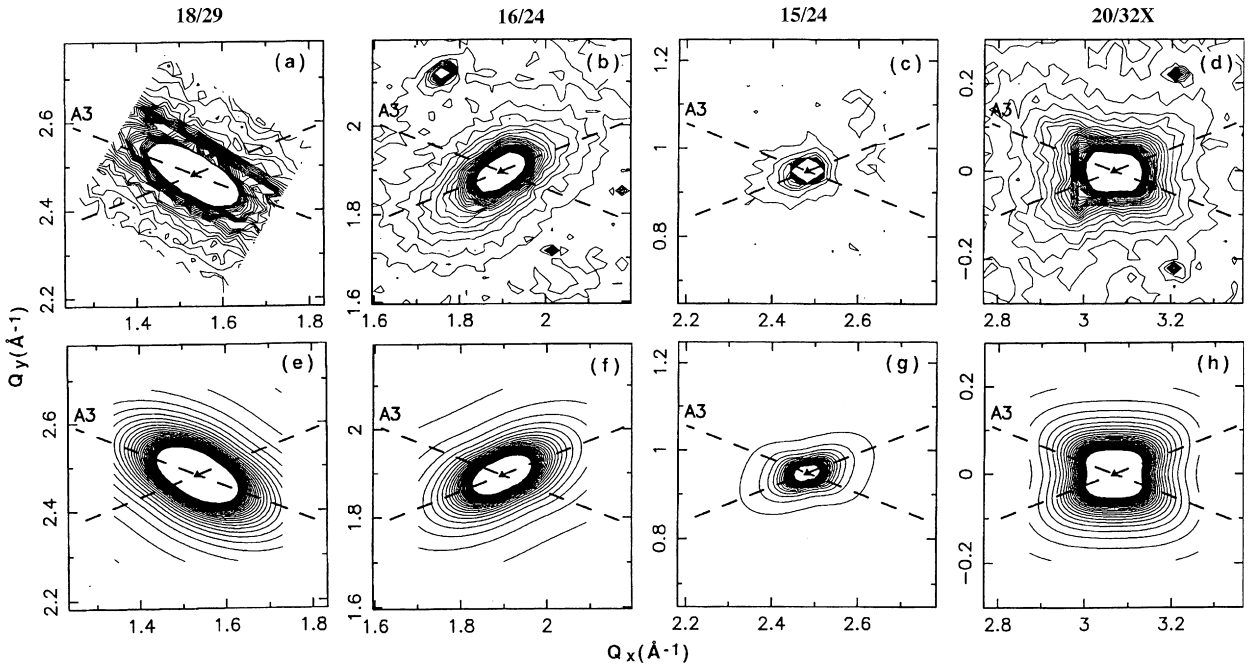

Fig. 5. Top panel (a–d): Iso-intensity contour plots measured by elastic neutron scattering around different Bragg peaks in the i-AlPdMn phase at room temperature. The indices are given in the N/M notation and refer to Fig. 3. All contour lines are on the same scale. Bottom panel (e–h): Simulation of the diffuse scattering using as a single parameter the K2/K1 ratio equal to −0.52. The dashed lines indicate directions parallel to 3-fold axes.

and experiment. A quantitative agreement was also achieved by comparing the intensity decay observed along different directions and various Bragg peaks.

The diffuse scattering was measured on an absolute scale using both neutron and X-ray scattering. In the case of X-ray, in order to minimize parasitic scattering, the measurement is carried out on a large sample (1 cm in diameter), in reflection geometry, the sample being under vacuum. To put the result on an absolute scale we used either a calibrated Al powder, or a combined precise measurement of the direct beam intensity and of the aperture of the receiving slits [29]. Both normalization procedures lead to the same result. The absolute scale measurement is particularly important in the case of X-ray scattering. Indeed it allows for the evaluation of the different contributions to the signal: TDS, Compton scattering and PDS. From this absolute scale measurement, the values of the two elastic constants K1 and K2 were evaluated. Values of $K1/k_BT$ equal to 0.1 and $K2/k_BT$ equal to -0.052 atom^{-1} have been found [32]. As already stated, this measurement procedure is completely analogous to the determination of elastic constants or phonon dispersion using X-ray diffuse scattering [24,25]. The static character of the speckle pattern obtained when using coherent X-ray scattering to measure the diffuse scattering is also a way to distinguish the signal from the one arising from phonons [33].

The temperature dependence of the diffuse scattering has been studied by neutron scattering between 25 °C and 770 °C, using a triple axis instrument to suppress the phonon contribution. The T dependence of the diffuse scattering displays a rather conter-intuitive behavior, since the diffuse scattering intensity diminishes as T is increased [34]. All the observed data can be interpreted assuming that the phason elastic constant increases as T increases. One observes in fact a phason 'softening' as the temperature is decreased, the phason modes being the result of pre-transitional fluctuations. This is what is expected from the Landau theory of phase transition [21,22] with in the present case pre-transitional fluctuation towards a phase of symmetry D_{3d}.

So far we have only considered the static behavior of phason modes in quasicrystals. As explained in the introduction, the hydrodynamic theory predicts that phason modes are collective diffusive modes. It means that a phason fluctuation follows an exponential time decay, with a characteristic time scale τ going as q^{-2} where q is the phason mode wavevector. This is equivalent to a characteristic time scale going like λ^2, where λ is the phason mode wavelength. At the thermodynamical equilibrium, phason modes of all wavelengths are present in the quasicrystal following a Boltzmann distribution. Since a distortion of the cut space results in atomic rearrangements, a phason mode with a wavevector $\mathbf{q}$ results in correlated atomic rearrangements. Suppressing this fluctuation requires atomic diffusion on long distances, explaining why the decay time should go as λ^2. The dynamics of phason fluctuations has been studied using coherent X-ray scattering and X-ray photo-correlation spectroscopy. The methods and results are presented in the section by F. Livet and M. Sutton ([35], this issue). At room temperature the speckle pattern is static [33] whereas it is time dependent above 500 °C. The diffusive character of the phason modes has been demonstrated and the phason diffusion constant defined as $q^{-2} = D_{\text{phason}}\tau$ is found to be equal to 2.2×10^{-18} m^2 s^{-1} [36,37].

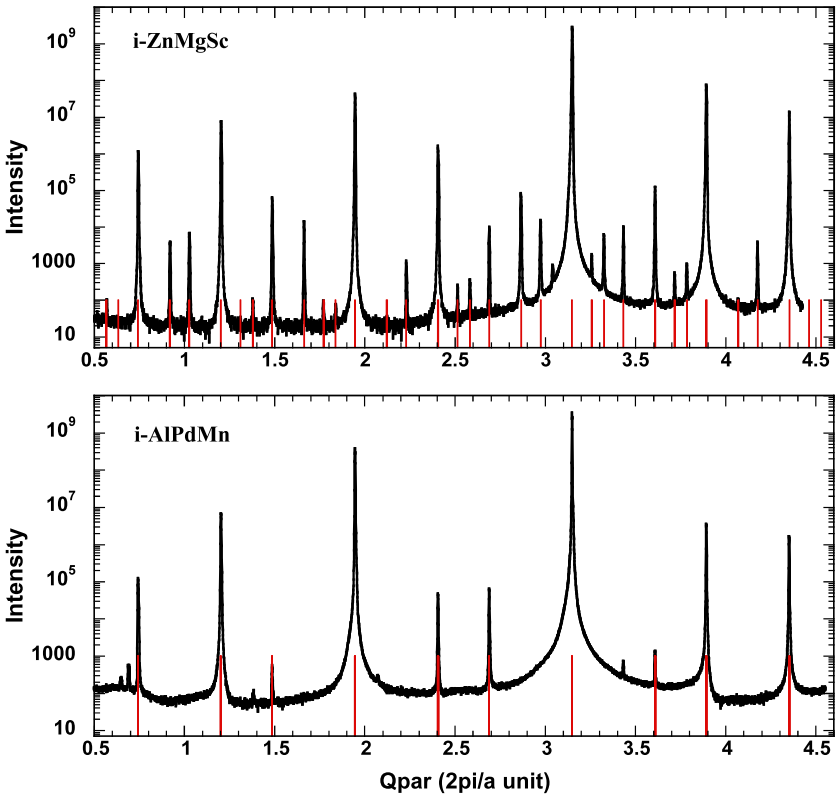

Fig. 6. Comparison of the scattered intensity signal measured in the i-ZnMgSc and i-AlPdMn phases along a 2-fold axis. The amount of diffuse scattering is lower in i-ZnMgSc and the number of large Q_{per} weak reflections larger. Bars stand for the calculated Bragg peak positions considering a maximum Q_{per} value of 7 in i-ZnMgSc and 2.5 in i-AlPdMn (from [38]).

Diffuse scattering studies have been carried out on most other icosahedral quasicrystalline phases. The main result is that for all known quasicrystals, even the so-called 'perfect' ones, phason diffuse scattering is observed. The shape anisotropy (related to the ratio of the K1 and K2 phason elastic constants), and the amount of diffuse scattering (related to the magnitude of the phason elastic constants) is however strongly sample dependent. Of particular interest is the comparison carried out between the i-ZnMgSc and the 1/1 cubic ZnSc approximant. Whereas the diffuse scattering observed in the ZnSc cubic approximant can be fully interpreted by a TDS contribution, in the i-ZnMgSc quasicrystal there is a supplementary contribution to the diffuse scattering arising from phason modes [38,39]. We stress here again the importance of having carried out absolute scale measurements, which allowed for an exact computation of the TDS contribution. This result demonstrates that the phason diffuse scattering is related to the long range quasiperiodic order and not to the local order, since both the QC and its approximant share the same large atomic cluster. It was also found that the amount of diffuse scattering in the i-ZnMgSc phase is much smaller than in the i-AlPdMn one. As a consequence phason elastic constants are larger and the phason Debye Waller factor is much smaller in the i-ZnMgSc phase than in the i-AlPdMn one. As a result a much larger number of high Q_{per}, weak reflections are observed in the diffraction pattern of the i-ZnMgSc phase than in the one of the i-AlPdMn phases. In fact the i-ZnMgSc diffraction pattern can only be indexed by considering reflections having a perpendicular component of their 6D reciprocal wave-vector up to 7, whereas the higher value of the Q_{per} component experimentally observed in i-AlPdMn is 2.5 as shown in Fig. 6.

4. Lattice dynamics of quasicrystal and approximants

Once the structure of the quasicrystal is best understood, one may raise the question of their physical properties. In particular, does the long range quasicrystalline order bring in new physical properties? We have already seen in Section 3 that phason modes are characteristics of the aperiodic long range order, but what about electronic and dynamical properties? Because of the lack of translational symmetry, the usual tools of solid state physics such as the Bloch wave expansion do not apply anymore. It is only for 1-dimensional systems that exact calculation could be carried out in aperiodic systems. In this case it has been shown that the wavefunction for electrons (and similarly the eigen-vectors for lattice dynamics) are critical: they are neither extended as in a simple structure, nor localized as in a random structure [40]. They rather show a power-law decay and self-similarity related to the long range aperiodic order. In 2D and 3D only simulations on large periodic approximant have been carried out. Although not proven rigorously, it has been conjectured that the wavefunctions

is critical for some energy range [2,41]. The similarity of local environments and their distribution in space plays a crucial role for this power-law decay. Proving experimentally this critical behavior is most likely very difficult. Indirect evidences have been looked for in the electronic transport properties or measurement of the electronic density of state. One must admit that no clear conclusion has been achieved in this field. Whereas the Al-based quasicrystals display a pseudo-gap at the Fermi level and a low conductivity as compared to their constituent, this is not the case for the binary Cd-based quasicrystal for which a rather metallic behavior is observed.

Much effort has been also dedicated to the study of the lattice dynamics of quasicrystals. Theoretical studies have shown that for a 3D system one may expect three regimes: for long wavelength excitations, acoustic phonons are well defined propagating excitations. This is the only regime for which an un-ambiguous definition of the phonon mode can be given. For higher energies, the eigen-vectors might correspond to critical states, with the importance of local configurations [2, 42,43]. The 'phonon' excitation spectrum is best studied using inelastic neutron or X-ray scattering. The measured function $S(Q, E)$ will display a well defined peak as a function of $\mathbf{Q} = \mathbf{Q}_{\text{Bragg}} + \mathbf{q}$ and the energy transfer E, if a phonon with wave vector $\mathbf{q}$ and energy E exists in the system. Moreover, there are selection rules, which will enhance or annihilate some of the contributions. Finally, the intensity distribution is related to the Fourier transform of the pattern of vibration and thus somehow to the eigen-vectors of the system. This tool is thus unique and very sensitive.

Although the quasicrystal is non-periodic, the quasiperiodic long range orders allows one to define pseudo-Brillouin zones [44–46], which are quasi-periodically stacked around the strong Bragg peaks taken as zone center. Close to the strong Bragg peaks a well defined acoustic excitation is expected, and has indeed been observed experimentally.

The most detailed study so far has been conducted in the Zn(Mg)Sc system [47]. Indeed the discovery of a binary CdYb quasicrystal by the group of An-Pang Tsai in 2000 [7] has been a real breakthrough in the field which led to the first accurate structural determination of a quasicrystal as shown in Section 2. The stable binary i-Cd–Yb [7] icosahedral (i-) phase and the isostructural i-Zn–Mg–Sc [48] phase are particularly interesting in that respect since both a quasicrystal and a periodic approximant can be synthesized, with almost the same chemical composition [8,9]. The QC and its approximant thus offer a unique possibility of comparing the respective effect of the short range order (RTH units) and long range order (periodic versus quasiperiodic) on physical properties and on their lattice dynamics.

The inelastic scattering function $S(\mathbf{Q}, E) = S(\mathbf{Q}_{\text{Bragg}} + \mathbf{q}, E)$ has been measured by inelastic neutron scattering and X-ray scattering for both the QC and its 1/1 approximant. Some results are reported in Fig. 7 for transverse excitations. The extracted dispersion relation has an overall similar shape in both cases. In particular there is an acoustic branch, separated by a pseudo-gap from an optical excitation located around 14 meV. However significant differences are also observed. In particular the width of the pseudo-gap is larger and better defined in the 1/1 approximant than in the quasicrystal: this is visible in the dispersion relation but also in the intensity distribution. The second difference is a slightly higher energy for the 1/1 approximant optical modes than for the quasicrystal. This is the first clear evidence of a difference in physical properties and in particular lattice dynamics between an approximant and a quasicrystal.

These differences can be qualitatively interpreted using the concept of PZB previously introduced in the case of the quasicrystal. Indeed, as already explained the important PZB have rather small wavevector and corresponds to Bragg peaks having a high Q_{per} component. As a result the single ZB in the 1/1 approximant is replaced by two PZB shown as vertical dashed line in Fig. 7. It means that the 'efficiency' of the phonon wave Bragg reflection is smaller in the QC than in the 1/1 approximant. This is also confirmed by the intensity of the corresponding Fourier components which is smaller in the QC than in the 1/1 approximant. As a result, the pseudo-gap between the acoustic and optical excitation is smaller in the QC.

Finally similarly to other quasicrystals one observes a rapid broadening of the acoustic excitations for q larger than 0.3 Å^{-1} in both cases, although excitations in the QC are slightly broader than the ones in the 1/1 approximant.

The above experimental results have been compared with simulations on realistic atomic models. This is possible thanks to the detailed knowledge of the atomic structure. To model the interactions in the Zn–Sc system, oscillating pair potentials which have been fitted against ab-initio data [49] have been used and are shown in Fig. 8. Note that the minimum of Sc–Sc distances is larger than the Zn–Zn as expected for those two atoms with different sizes. The right panel of Fig. 8 illustrates the quality of the force matching fitting using oscillating pair potentials.

To compute the dynamical response of the QC, we needed a unique realization of the structure with periodic boundary condition. A 3/2 cubic approximant which contains 32 clusters in the unit cell, and has lattice parameter equal to 36.13 Å has been used. A binary decoration Zn–Sc, based on the related i-CdYb atomic structure [10] and on the ternary 2/1 MgScZn [50] has been used. The modeling was achieved by positioning the RTH units on the vertices of the so called canonical cell tiling [51] of the 3/2 approximant with a decoration procedure as described in [52]. Ambiguous atomic sites positions were determined by total energy minimization. As for the 1/1 approximant, the tetrahedral orientation where obtained by a molecular dynamic annealing followed by a quench. Induced deviations from icosahedral symmetry of the successive shells around the tetrahedron are a crucial parameter. The resulting model has a composition $Zn_{2528}Sc_{456}$, contains 2984 atoms per unit cell and presents a diffraction pattern which compares well to the QC one. For the 1/1 approximant a supercell was also used in order to take into account the random orientation of the central tetrahedron experimentally observed at room T.

Using these models and the fitted pair potentials the inelastic response function $S(\mathbf{Q}, E)$ has been calculated either in the harmonic approximation and by direct diagonalization of the dynamical matrix, or from atom trajectories generated by room temperature molecular dynamics, using the method described in Ref. [53]. The latter approach is not relying on the

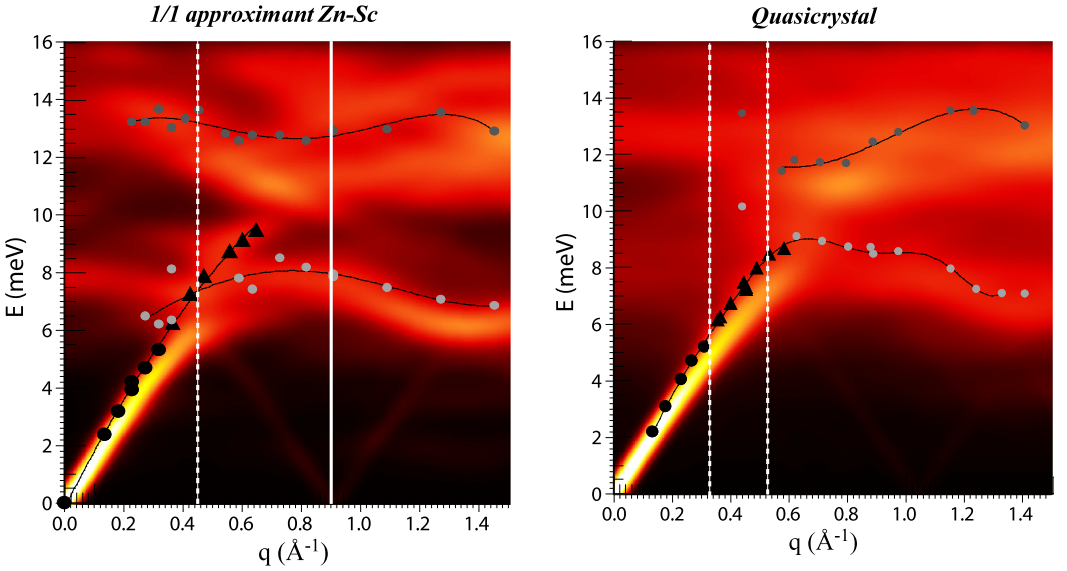

Fig. 7. Transverse excitations: comparison between the measured dispersion relation (symbols) and the simulated response function $S(Q, E)$ (temperature color-coded) in the 1/1 approximant (left panel) and the quasicrystal (right panel). The figure shows the intensity distribution of the simulated response function on a temperature color-coded scale. The experimental positions of the excitations, as measured by neutron inelastic scattering, are shown by symbols: the black closed circles and triangles stand for the acoustic signal whereas other symbols correspond to optical excitations. Black triangles indicate the q positions for which the normalized acoustic intensity is no longer constant. Vertical white dashed lines indicate the position of the (pseudo) Brillouin zone boundaries. The simulation reproduces both the general trend and the differences observed between the QC and its approximant.

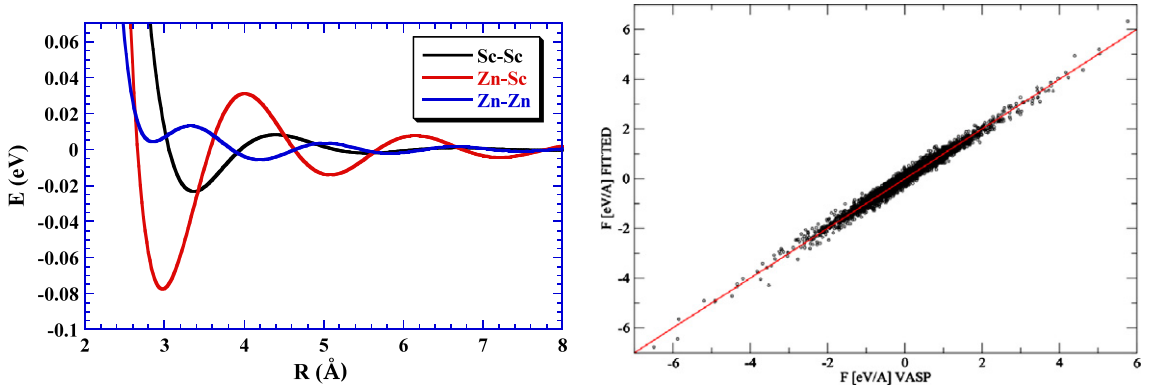

Fig. 8. Left panel: Radial dependence of the energy of the oscillating pair potentials used in the simulation of the ZnSc approximant and QC dynamics. Right panel: Force matching fit, showing the forces calculated with ab-initio (VASP) as a function of the one calculated with the oscillating pair potentials. There is a very good agreement.

harmonic approximation, which might have been an issue due to suspected shallow minima in the energy landscape related to tetrahedron librations. However, the two approaches did not show any significant differences.

Fig. 7 displays the calculated $S(\mathbf{Q}, E)$ in the transverse geometry for both the approximant and the quasicrystal. The calculation is temperature color coded, and does not include the term $n(E)/E$ (where $n(E)$ is the Bose occupation factor), so that the acoustic mode presents a constant intensity. In both figures, the simulation has been convoluted with a Gaussian distribution with FWHM of 1 meV. Although the calculated transverse acoustic excitations are slightly too soft, the main features are nicely reproduced by the calculation: acoustic modes and pseudo gap, high energy optical excitations, low lying optical excitation in longitudinal geometry. Even the detailed differences between the QC and the approximant are reproduced: a larger pseudogap in the approximant than in the QC, the interaction with an optical excitation around 7.5 meV at the BZB in transverse geometry for the approximant, lower positions of the optical bands in the QC than in the approximant.

Not only the dispersion relations are matched by the calculation, but also the intensity distribution is qualitatively well reproduced.

We insist on the fact that the very good quantitative agreement for the intensity distribution is exceptional. Indeed, this means that the simulation reproduces correctly the eigen-vectors or the pattern of vibrations of both the QC and its 1/1 approximant. In fact, there are extremely few examples, even for simpler systems, for which such a quantitative comparison has been achieved.

This has been only possible because a detailed structure analysis is available on one hand and because the oscillating pair potentials are a good approximation of the Hamiltonian on the other hand. This is certainly because: (i) there is a strong size effect with a large and small atom; (ii) the oscillation of the pair potential are a good approximation for the electronic stabilization and in particular the so-called Friedel oscillations.

Now that the simulations are validated on a very firm basis, it is possible to analyze in more detail the results. In particular it is interesting to check the eventual role of clusters; are they cluster modes? Is the quasiperiodic order bringing in a signature? What about critical modes? This is a difficult question which is under study.

Nevertheless, this study demonstrates that detailed information on the lattice dynamics can now been simulated and analyzed. This opens the route for studies in metallurgy where complex phases are frequently encountered.

5. Conclusion

We have shown that tremendous progress has been achieved since the discovery of quasicrystals, and that large scale facilities have delivered key data for this understanding. Thanks to the discovery of a binary quasicrystals and the use of synchrotron data, a detailed structural analysis has been carried out. The effect of phason fluctuations, excitations which are specific to quasicrystal, has also been studied using X-ray or neutron diffuse scattering measurement. Finally the lattice dynamics studied by inelastic neutron and X-ray scattering has brought in evidence for the difference between the quasicrystal and its approximant. The simulation, using oscillating pair potentials, is in very good qualitative and quantitative agreement. The fascinating question of how and why the quasiperiodic long range order sets in can now be addressed.

References

[1] D. Shechtman, I. Blech, D. Gratias, J.W. Cahn, Phys. Rev. Lett. 53 (1984) 1951–1953.
[2] T. Janssen, G. Chapuis, M. de Boissieu, Aperiodic Crystals. From Modulated Phases to Quasicrystals, Oxford University Press, Oxford, 2007, 466 pp.
[3] I.R. Fisher, Z. Islam, A.F. Panchula, K.O. Cheon, M.J. Kramer, et al., Phil. Mag. B 77 (1998) 1601.
[4] S.W. Kycia, A.I. Goldman, T.A. Lograsso, D.W. Delaney, D. Black, et al., Phys. Rev. B: Condens. Matter 48 (1993) 3544–3547.
[5] T. Jach, Y. Zhang, R. Colella, M. de Boissieu, M. Boudard, et al., Phys. Rev. Lett. 82 (1999) 2904–2907.
[6] J. Gastaldi, S. Agliozzo, A. Letoublon, J. Wang, L. Mancini, et al., Phil. Mag. B 83 (2003) 1–29.
[7] A.P. Tsai, J.Q. Guo, E. Abe, H. Takakura, T.J. Sato, Nature 408 (2000) 537–538.
[8] C.P. Gomez, S. Lidin, Angew. Chem. Int. 40 (2001) 4037–4039.
[9] C.P. Gomez, S. Lidin, Phys. Rev. B 68 (2003) 024203, 024201–024209.
[10] H. Takakura, C.P. Gomez, A. Yamamoto, M. de Boissieu, A.P. Tsai, Nature Mater. 6 (2007) 58–63.
[11] A.W. Overhauser, Phys. Rev. B 3 (1971) 3173–3182.
[12] R. Currat, T. Janssen, Sol., Stat. Phys. 41 (1988) 201–302.
[13] P.A. Kalugin, A.Y. Kitaev, L.S. Levitov, JETP Lett. 41 (1985) 145–149.
[14] P. Bak, Phys. Rev. Lett. 54 (1985) 1517–1519.
[15] T.C. Lubensky, S. Ramaswamy, J. Torner, Phys. Rev. B 32 (11) (1985) 7444–7452.
[16] V. Elser, Phys. Rev. Lett. 55 (1985) 1730.
[17] M. de Boissieu, R. Currat, S. Francoual, Phason modes in aperiodic crystals, in: T. Fujiwara, Y. Ishii (Eds.), Handbook of Metal Physics: Quasicrystals, Elsevier Science, Amsterdam, 2008, pp. 107–169.
[18] P.A. Kalugin, A.Y. Kitaev, L.S. Levitov, J. Phys. (France) Lett. 46 (1985) L601.
[19] M.V. Jaric, D.R. Nelson, Phys. Rev. B 37 (1988) 4458–4472.
[20] P.M. Chaikin, T.C. Lubensky, Principles of Condensed Matter Physics, Cambridge University Press, Cambridge, 2000, 699 pp.
[21] Y. Ishii, Phys. Rev. B 39 (16) (1989) 11862–11871.
[22] Y. Ishii, Phil. Mag. Lett. 62 (1990) 393–397.
[23] Y. Ishii, Phys. Rev. B 45 (1992) 5228–5239.
[24] J. Laval, C. R. Acad. Sci. Paris 207 (1938) 169.
[25] J. Laval, Bull. Soc. France Miner. 62 (1939) 137.
[26] P. Olmer, Acta Cryst. 1 (1948) 57.
[27] H. Curien, Acta Cryst. 5 (1952) 393.
[28] C.B. Walker, Phys. Rev. B 103 (1956) 547–557.
[29] B.E. Warren, X-Ray Diffraction, Dover, New York, 1990 (republication of Addison–Wesley, 1969).
[30] R.W. James, The Optical Principles of the Diffraction of X-Rays, Oxbow Press, 1962, p. 664.
[31] M. de Boissieu, M. Boudard, B. Hennion, R. Bellissent, S. Kycia, et al., Phys. Rev. Lett. 75 (1995) 89.
[32] A. Létoublon, M. de Boissieu, M. Boudard, L. Mancini, J. Gastaldi, et al., Phil. Mag. Lett. 81 (2001) 273–283.
[33] A. Letoublon, F. Yakhou, F. Livet, F. Bley, M. de Boissieu, et al., Europhys. Lett. 54 (2001) 753–759.
[34] M. Boudard, M. de Boissieu, A. Létoublon, B. Hennion, R. Bellissent, et al., Europhys. Lett. 33 (3) (1996) 199–204.
[35] F. Livet, M. Sutton, C. R. Phys. 13 (3) (2012) 227–236, in this issue.
[36] S. Francoual, F. Livet, M. de Boissieu, F. Yakhou, F. Bley, et al., Phys. Rev. Lett. 91 (2003) 225501, 225501–225504.
[37] S. Francoual, F. Livet, M. de Boissieu, F. Yakhou, F. Bley, et al., Phil. Mag. 86 (6–8) (2006) 1029–1035.
[38] M. de Boissieu, S. Francoual, Y. Kaneko, T. Ishimasa, Phys. Rev. Lett. 95 (2005) 105503.
[39] S. Francoual, Phonon and phason in icosahedral quasicrystals and in their 1/1 periodic approximant, PhD thesis, Université Joseph Fourier, 2006.
[40] J.P. Lu, T. Odagaki, J. Birman, Phys. Rev. B 33 (1986) 4809.
[41] T. Fujiwara, Y. Ishii, Physics of Quasicrystals, Elsevier Science, 2007.
[42] J. Los, T. Janssen, J. Phys.: Condens. Matter 2 (1990) 9553–9566.
[43] J. Hafner, M. Krajci, J. Phys.: Condens. Matter 5 (1993) 2489–2510.
[44] K. Niizeki, J. Phys A: Math. Gen. 22 (1989) 4295–4302.
[45] K. Niizeki, T. Akamatsu, J. Phys.: Condens. Matter 2 (12) (1990) 2759–2771.
[46] K. Niizeki, T. Akamatsu, J. Phys.: Condens. Matter 2 (33) (1990) 7043–7047.
[47] M. de Boissieu, S. Francoual, M. Mihalkovic, K. Shibata, A.Q.R. Baron, et al., Nature Mater. 6 (2007) 977–984.

[48] Y. Kaneko, Y. Arichika, T. Ishimasa, Phil. Mag. Lett. 81 (2001) 777–787.
[49] M. Mihalkovic, C.L. Henley, M. Widom, G. Panchapakesan, 2007, submitted for publication.
[50] Q.S. Lin, J.D. Corbett, J. Am. Chem. Soc. 128 (2006) 13268–13273.
[51] C.L. Henley, Phys. Rev. B 43 (1991) 993–1020.
[52] M. Mihalkovic, M. Widom, Phil. Mag. 86 (2006) 519–527.
[53] T. Rog, K. Murzyn, K. Hinsen, G.R. Kneller, J. Comput. Chem. 24 (2003) 657–667.